Ocular Anterior Segment Biometry and High-Order Wavefront Aberrations During Accommodation

Yimin Yuan,[1] Yilei Shao,[1] Aizhu Tao,[1] Meixiao Shen,[1] Jianhua Wang,[2] Guohua Shi,[3] Qi Chen,[1] Dexi Zhu,[1] Yan Lian,[1] Jia Qu,[1] Yudong Zhang,[3] and Fan Lu[1]

[1]School of Ophthalmology and Optometry, Wenzhou Medical University, Wenzhou, China
[2]Bascom Palmer Eye Institute, University of Miami Miller School of Medicine, Miami, Florida
[3]Institute of Optics and Electronics, Chinese Academy of Sciences, Chengdu, China

Correspondence: Fan Lu, School of Ophthalmology & Optometry, Wenzhou Medical University, 270 Xueyuan West Road, Wenzhou, Zhejiang, China, 325027; lufan@mail.eye.ac.cn.
Yudong Zhang, The Key Laboratory on Adaptive Optics, Chinese Academy of Sciences, Institute of Optics and Electronics, Chinese Academy of Sciences, Chengdu, China, 610209; ydzhang@ioe.ac.cn.

YY and YS contributed equally to the work presented here and should therefore be regarded as equivalent authors.

Submitted: February 19, 2013
Accepted: September 9, 2013

Citation: Yuan Y, Shao Y, Tao A, et al. Ocular anterior segment biometry and high-order wavefront aberrations during accommodation. *Invest Ophthalmol Vis Sci*. 2013;54:7028–7037. DOI: 10.1167/iovs.13-11893

Purpose. We investigated the relationships between the ocular anterior segment biometry and the ocular high-order aberrations (HOAs) during accommodation by combined ultralong scan depth optical coherence tomography (UL-OCT) and wavefront sensor.

Methods. We enrolled 35 right eyes of young healthy subjects (21 women and 14 men; age, 25.6 ± 3.1 years; spherical equivalent refractive error, −0.41 ± 0.59 diopters [D]). A custom-built UL-OCT and a wavefront sensor were combined. They were able to image the ocular anterior segment and to measure the HOAs during accommodation. The differences in the biometric dimensions and in the HOAs between the nonaccommodative and accommodative states were compared, and the relationships between them were investigated.

Results. Compared to the nonaccommodative condition, anterior chamber depth, pupil diameter, and radii of the crystalline lens surface curvatures decreased significantly, while the lens thickness and root-mean-square of high-order aberration (HORMS) of fixed 3-mm pupil size increased under the accommodative stimulus ($P < 0.01$). A negative correlation was found between the change in the radius of the lens anterior surface curvature and the change in HORMS ($r = -0.370$, $P = 0.014$). For nonaccommodative and accommodative conditions, HORMS for a fixed pupil size was correlated negatively with pupil diameter ($r = -0.532$ and -0.801, respectively, $P < 0.01$).

Conclusions. The anterior segment biometry and the HOAs changed significantly during accommodation. The increase in HOAs mainly was due to the increased convexity of the anterior surface of the lens during accommodation. Contraction of the pupil may help to decrease HOAs.

Keywords: accommodation, optical coherence tomography, aberrations, anterior segment, crystalline lens, pupil

Accommodation is the dynamic process by which the human eye focuses on nearby objects by increasing the optical power.[1] The purpose of accommodation is to form a clear optical image on the retina; however, the optical performance of the human eye during this process is not ideal. First, the change in dioptric power of the eye, that is, the accommodative response, is not equal to the demand. Accommodative lead and lag, and microfluctuations often occur,[2] and accommodation-induced astigmatism also is common.[3,4] These phenomena lead to a defocused retinal image. Second, high-order aberrations (HOAs) of the eye are altered during accommodation. For instance, the spherical aberration changes from a positive value to a negative one,[5–8] while the direction of the coma change varies among subjects.[6–8] Furthermore, the root-mean-square (RMS) of HOAs (HORMS) increases during accommodation, even though there is a large variation between individuals.[9,10] In other words, low-order aberrations and HOAs of the eye change significantly during accommodation. These changes, in turn, alter the optical image quality on the retina.

While accommodation compensates for retinal defocus, it also induces changes in ocular wavefront aberrations. Thus, to understand the regulatory mechanisms of image quality control in the human eye, it is necessary to explore the factors that alter ocular aberrations. According to the theories of von Helmholtz[1] and Fincham,[11] there is a significant change in the curvature of the crystalline lens surface during accommodation, accompanied by an increase in lens thickness and a decrease in anterior chamber depth. Because there is little evidence of changes in corneal shape,[12,13] the changes in ocular aberrations with accommodation may be due to mainly the reshaping of the crystalline lens. However, even though the relationship between the aberrations and accommodation has been established, there is little direct in vivo evidence that demonstrates the connection between wavefront aberrations and the morphologic parameters of the ocular anterior segment during accommodation.

Optical coherence tomography (OCT) is a rapid and noninvasive method for imaging the anterior eye.[14,15] Recently, we have developed a custom-built, high-resolution, spectral-domain OCT instrument with ultralong scan depth (UL-OCT).[16,17] With this instrument, it is possible to quantify the dimensional changes of the anterior segment during accommodation on a micrometer scale. In our previous work, the UL-OCT instrument and a custom-developed Hartmann-Shack

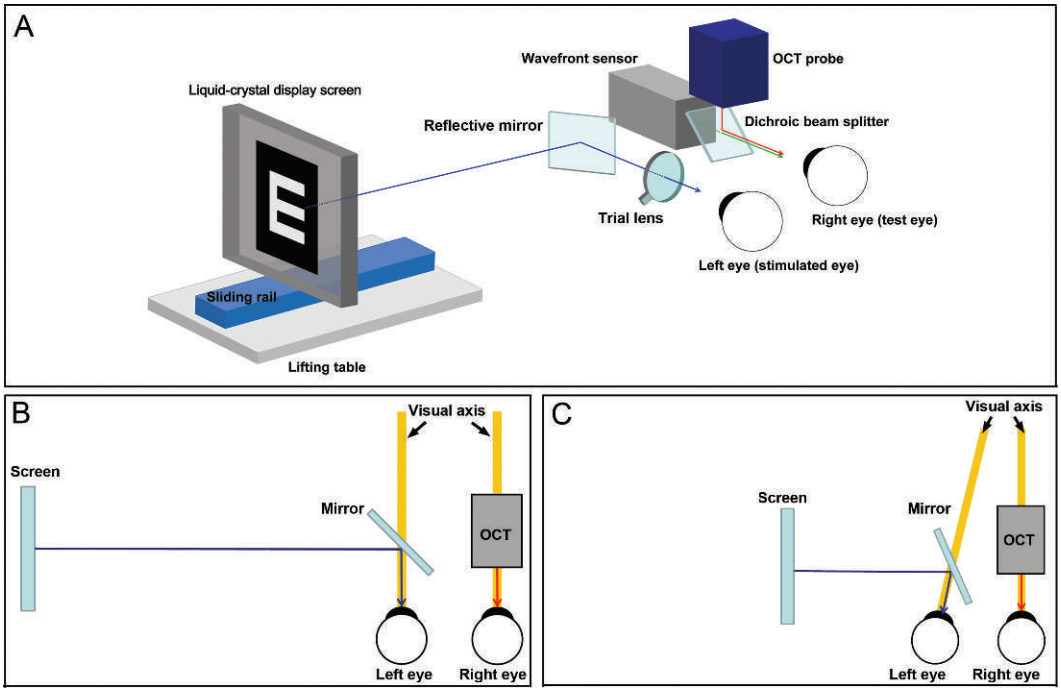

Figure 1. Diagram of the combined UL-OCT probe and wavefront sensor, and fixation target system. (**A**) The wavefront sensor and probe of the UL-OCT instrument were combined. A liquid-crystal display screen was held on a lifting table, showing a white "E" in a black background field. The screen was mounted on a sliding rail that was adjusted to produce different accommodative stimuli. A reflected mirror was placed in the front of the left eye to image the target. Trial lenses were used to compensate for refractive error. (**B**) In the nonaccommodative state, the visual axes of the two eyes were parallel. (**C**) In the accommodative state, the mirror in front of the left eye was adjusted so that convergence occurred in the left eye, but the right eye was aligned with the UL-OCT system.

wavefront sensor were combined.[18] The integrated system succeeded in obtaining anterior segment biometry and ocular wavefront aberrations. The present study aimed to investigate the relationship between ocular anterior segment biometry and high-order wavefront aberrations during accommodation.

Subjects and Methods

Subjects

The participants were students or staff of Wenzhou Medical University. After screening, 35 healthy young subjects (21 women and 14 men; mean age ± SD, 25.6 ± 3.1 years; range, 20–33 years) were enrolled. In this study, only emmetropic and low myopic subjects were enrolled, because the refractive error may be related to ocular morphology, accommodative response, and wavefront aberrations. The mean spherical equivalent of the test eye was −0.41 ± 0.59 diopters (D; range, +0.50 to −2.38 D), with astigmatism <0.75 D. The difference in the spherical equivalent between the two eyes of each subject was <1.00 D. The best corrected visual acuity in each eye was 20/20 or better. No subjects had any abnormal ocular findings, or any history of ocular diseases, surgery, trauma, or contact lens wear. This study was approved by the research review board of Wenzhou Medical University. Informed consent was obtained from each subject, and all were treated in accordance with the tenets of the Declaration of Helsinki.

Instruments

Our combined custom-built, high-resolution, UL-OCT instrument, and custom-developed Hartmann-Shack wavefront sensor (Fig. 1) were used to image the anterior segment and record ocular HOAs. The combined probe was mounted on a modified slit-lamp platform. A dichroic beam splitter was used to combine the two measuring lights. Light (780 nm) from the wavefront sensor passed through the mirror, and the UL-OCT beam (840 nm), with a full-width at a half maximum bandwidth of 50 nm, was reflected at 45°. The UL-OCT system was described elsewhere[16] and demonstrated to have good repeatability for measuring the anterior segment of the eye during accommodation.[17] The A-line (depth scan) rate of the OCT system was 24,000 Hz, as determined by a charged-couple device (CCD) line scan camera (Aviiva-SM2010, 2048 pixels; Atmel, e2v, Inc., Elmsford, NY). The scan depth was 7.8 mm in air, with an axial resolution of 7.5 μm in tissue.[16] As detailed in our previous work,[17] the full range of the anterior segment of the eye can be imaged by analysis of both conjugated mirror images in UL-OCT. By placing the zero delay line at the front surface of the crystalline lens, both conjugated images were flipped and overlapped. With custom software, the raw images with mirror artifacts were processed and reconstructed to obtain the full-range anterior segment images with an equivalent scan depth of 15.6 mm. An x-y galvanometer pair served as a scanner and allowed us to align the scanning position at horizontal and vertical meridians. This function provided precise alignment for UL-OCT imaging.

The Hartmann-Shack wavefront sensor used near-infrared light with a wavelength of 780 nm. This instrument had a 32 × 32 microlens array and captured 20 images per second. It was well calibrated, and the repeatability was tested.[19] Before the procedure, we also tested the repeatability of the wavefront sensor by measuring 10 subjects twice with accommodation relaxed. The mean values and standard deviations of the Zernike coefficients are shown in Table 1.

Table 1. Repeated Measurements of the HORMS and Zernike Coefficients in Unaccommodated Eyes

	Visit 1	Visit 2	Difference	*P* Value
HORMS	0.103 ± 0.072	0.111 ± 0.063	0.007 ± 0.017	0.33
SA	0.028 ± 0.038	0.028 ± 0.030	−0.001 ± 0.009	0.88
Coma	0.085 ± 0.065	0.096 ± 0.058	0.011 ± 0.015	0.14
Trefoil	0.032 ± 0.021	0.026 ± 0.018	−0.005 ± 0.008	0.16

Measurements were made in unaccommodated eyes over a fixed 3.0-mm pupil diameter ($n = 10$ eyes). Units are given in micrometers. SA, spherical aberration.

Experimental Procedures

The study was conducted in a consulting room that was kept completely dark. Measurements were taken on the right eye while the subjects fixed far and near targets with the left eye. No mydriatics were used. The subject sat in front of the probe with his/her chin on the chin rest and forehead against the forehead rest. By subjective refraction, trial lenses were placed in front of the left eye so that the refractive error of the left eye was corrected. A liquid-crystal display screen was set on a sliding rail on the left side of the combined probe, displaying a white Snellen letter "E" on a black background. The subject could view the letter via a mirror, which was mounted in front of the left eye (Fig. 1).

First, the letter "E" (size, 20/50) was 4.0 m away (0.25 D) from the trial lens in front of the left eye. The subject was instructed to view the target as clearly as possible. The right eye was aligned with the UL-OCT instrument by precisely centering the corneal apex, such that the specular reflection at vertical and horizontal meridians was visible. Therefore, the beam of the UL-OCT instrument was perpendicular to the iris plane. Then, an UL-OCT image of the anterior segment at the horizontal meridian was acquired immediately after a blink. Immediately after that, we blocked the beam from the UL-OCT probe, and then the ocular HOAs through the natural pupil of the right eye were recorded by the wavefront sensor. The time between the two measurements was approximately 5 to 10 seconds. After that, the fixation target was moved towards the probe and was set 33 cm away from the trial lens. The near target was designed for reading or near work. To prevent accommodative convergence in the right eye, the mirror in front of the left eye for viewing the target was adjusted (Fig. 1). This approach ensured that the right eye remained aligned during accommodation. The size of the "E" target was adjusted to maintain the same visual angle to the eye. After the subject could view the target clearly with the left eye, an UL-OCT image of the anterior segment and ocular HOAs were again recorded for the accommodative condition of the right eye.

Data Analysis

As described in a previous study,[20] raw UL-OCT images were exported and processed. We applied custom-developed software to semi-automatically segment and detect the boundaries of the cornea, iris, and crystalline lens. Thus, the positions of all interfaces in the UL-OCT images were semi-segmented. Then, the refraction correction algorithm based on Snell's principle was applied, and for each ray, we calculated the corrected positions of each interface.[21] The refractive indices of 1.387 for cornea,[22] 1.342 for anterior chamber,[23] and 1.408 for crystalline lens[24] were used in this algorithm at a wavelength of 840 nm. Dimensional parameters, including anterior chamber depth (ACD), pupil diameter (PD), lens thickness (LT), the radii of the anterior (ASC) and posterior (PSC) lens surface curvature, and anterior segment length (ASL), were obtained from the UL-OCT images (Fig. 2). The ASC and PSC were obtained using the least squares method to fit the lens surfaces with a circle equation. The radius of the fitted circle was defined as the radius of the lens surface curvature. The ASL was defined as the distance between the

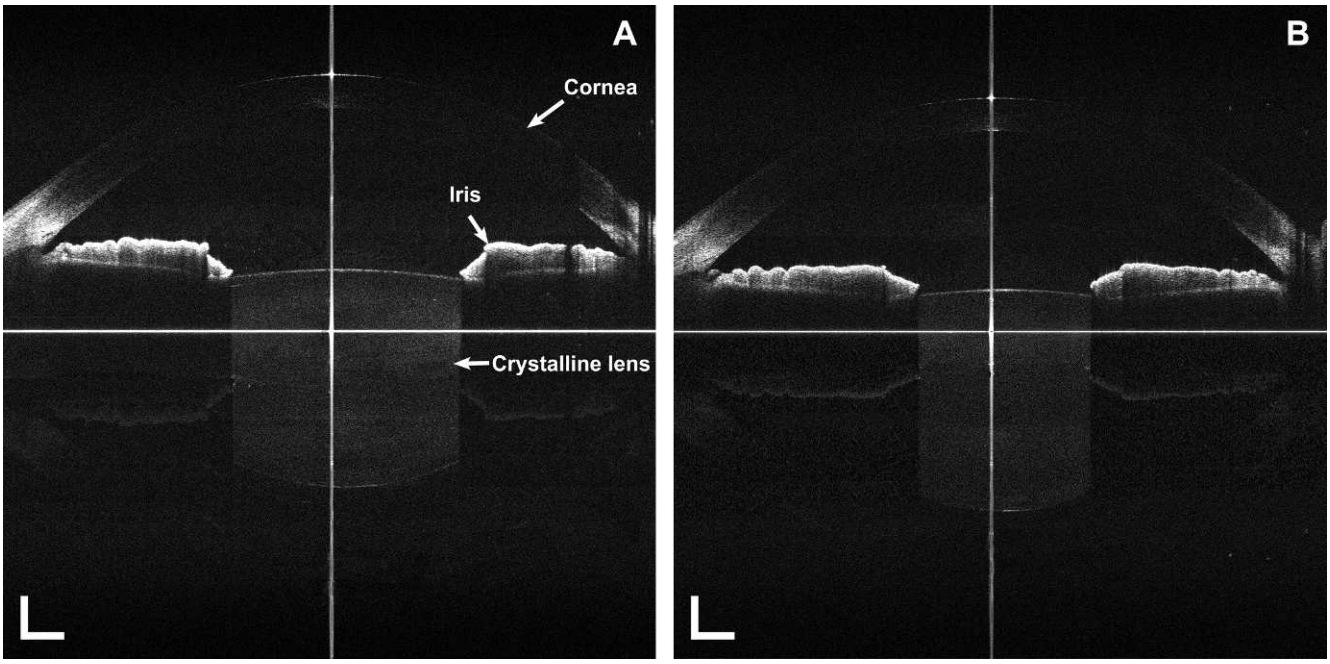

Figure 2. UL-OCT images in nonaccommodative and accommodative states. Images from a 30-year-old subject show the right eye in the (**A**) nonaccommodative and (**B**) accommodative states. The images were processed, reconstructed, and corrected at the anterior corneal and lens surfaces by the custom-developed algorithms. Note that the anterior surface of the lens became steeper during accommodation, with obvious pupil accommodative miosis. *Scale bars*: 1 mm.

Investigative Ophthalmology & Visual Science

Table 2. Changes in Biometric Dimensions, High-Order Aberrations, and Accommodative Response During Accommodation

Variable	Nonaccommodative State Mean	Nonaccommodative State SD	Accommodative State Mean	Accommodative State SD	*P* Value
PD, mm	5.786	0.832	4.872	0.899	<0.001
ACD, mm	3.040	0.252	2.925	0.256	<0.001
ASC, mm	12.326	1.136	9.988	0.955	<0.001
PSC, mm	5.735	0.681	5.400	0.681	<0.001
LT, mm	3.606	0.213	3.725	0.221	<0.001
ASL, mm	6.645	0.298	6.650	0.303	0.30
$HORMS_{natural}$, μm	0.412	0.116	0.439	0.075	0.07
$HORMS_{fixed}$, μm	0.085	0.078	0.249	0.115	<0.001
AR, D	−0.283	0.385	−2.106	0.461	<0.001

AR, accommodative response.

posterior surface of the central cornea and the posterior pole of the crystalline lens.

The wavefront data were obtained from the wavefront sensor. Zernike polynomials for natural pupil size in nonaccommodative and accommodative conditions were exported from the instrument, respectively. In addition, the natural pupil size varied among subjects and also varied during accommodation for individual subjects. The fixed 3.0-mm pupil diameter was selected to subtract the effect of pupil miosis, because it was smaller than the minimum natural pupil diameter of all subjects under the accommodative condition. Zernike polynomials for fixed 3.0-mm pupil diameter also were obtained in nonaccommodative and accommodative conditions, respectively. The layout of the polynomials was recommended by the Vision Science and Its Application (VSIA) Standards Taskforce team.[25] The Zernike coefficients from the third to the seventh order were used to calculate the RMS of ocular HOAs for natural pupil size ($HORMS_{natural}$) and for fixed 3.0-mm pupil diameter ($HORMS_{fixed}$).

For each subject, we computed the accommodative response from wavefront aberrations. The response was defined as the spherical equivalent error, based on the paraxial curvature matching of the wavefront map (Seidel defocus).[26] Thus, the residual refractive error (*M*) for each status was

$$M = \frac{-16\sqrt{3}c(2,0) + 48\sqrt{5}c(4,0) - 96\sqrt{7}c(6,0)}{-PD^2}, \quad (1)$$

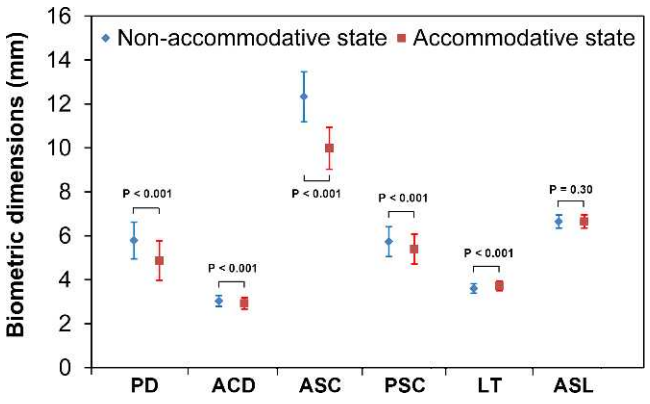

Figure 3. Biometric dimensions in nonaccommodative and accommodative states. All of the dimensional parameters, except ASL, changed significantly in the accommodative state compared to the nonaccommodative state. The *error bars* denote standard deviation.

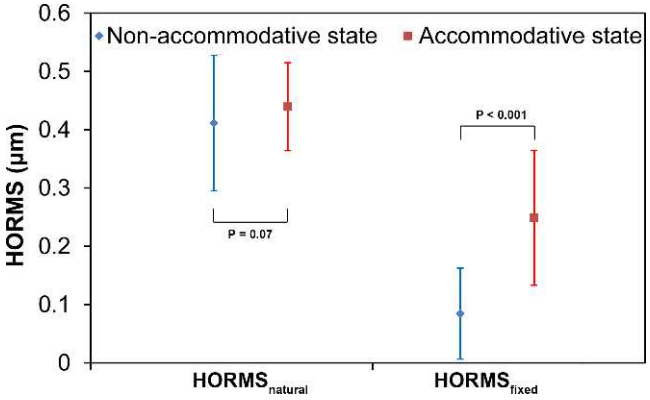

Figure 4. The HORMS in nonaccommodative and accommodative states. The $HORMS_{fixed}$ increased significantly in the accommodative state compared to the nonaccommodative state, while the $RMS_{natural}$ did not change. The *error bars* denote standard deviation.

where *M* presented in diopters, Zernike coefficients (*c*) in micrometers, and the pupil diameter (*PD*) in millimeters. The accommodative response at each accommodative stimulus was defined as the difference between the *M* and the subjective spherical equivalent refractive error.

Descriptive data were calculated as means ± SD. Data analyses were conducted using the Statistical Package for the Social Sciences (version 15.0; SPSS, Inc., Chicago, IL). Paired *t*-tests were applied to test the differences of biometric dimensions and HOAs between nonaccommodative and accommodative states. The relationship between biometric dimensions and HOAs was determined with Pearson correlation. Independent *t*-tests were used to test the differences of biometric dimensions and HOAs between the two subgroups. A *P* value of <0.05 was considered statistically significant.

Results

Accommodation-Induced Changes in Anterior Segment Biometry

During accommodation, ACD, PD, ASC, and PSC became significantly smaller (paired *t*-test, $P < 0.001$, Table 2, Fig. 3). Meanwhile, the LT significantly increased with accommodation (paired *t*-test, $P < 0.001$). However, the ASL remained unchanged between accommodative states (paired *t*-test, $P > 0.05$).

Accommodation-Induced Changes in Ocular HOAs

The $HORMS_{natural}$ showed no change during accommodation (paired *t*-test, $P > 0.05$, Table 2, Fig. 4). In contrast, $HORMS_{fixed}$ increased significantly under the accommodative condition compared to the nonaccommodative condition (paired *t*-test, $P < 0.001$, Table 2, Fig. 4). In addition, the accommodative response changed from 0.283 ± 0.385 to 2.106 ± 0.461 D during accommodation (paired *t*-test, $P < 0.001$, Table 2). Therefore, there was an accommodative lag for the 33-cm target (–0.894 ± 0.461 D).

Relationship Between Biometric Dimensions and Ocular HOAs

There was a negative correlation between the change in ASC and the change in $HORMS_{fixed}$ during accommodation (Pearson

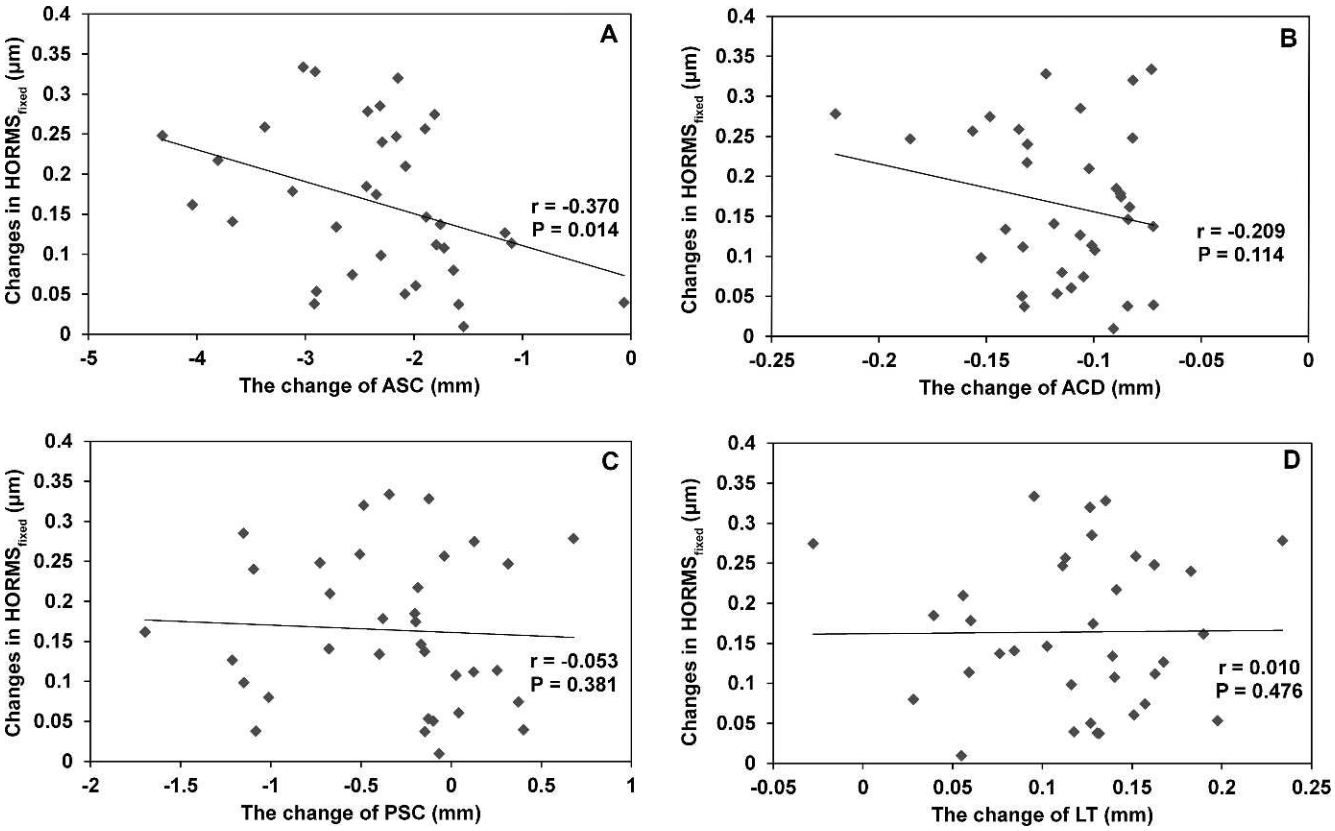

FIGURE 5. Relationships between the change in $HORMS_{fixed}$, and the changes in ASC, ACD, PSC, and LT during accommodation. There was a negative correlation between the change in (**A**) ASC and the change in $HORMS_{fixed}$, while the correlations between (**B**) ACD, (**C**) PSC, and (**D**) LT with $HORMS_{fixed}$ were weak.

correlation, $r = -0.370$, $P < 0.05$, Fig. 5A). In contrast, there were no significant correlations between the change in PSC, ACD, or LT and the change in $HORMS_{fixed}$ ($P > 0.05$, Figs. 5B–D). In addition, PD was correlated negatively with the $HORMS_{fixed}$ in nonaccommodative and accommodative states ($r = -0.532$ and -0.801, respectively, $P < 0.01$, Fig. 6).

The mean $HORMS_{natural}$ did not change significantly with accommodation. However, the individual changes in $HORMS_{natural}$ varied among subjects. Thus, we divided the subjects into two subgroups according to the tendencies of changes in $HORMS_{natural}$. Group A was composed of subjects ($n = 20$) with increased $HORMS_{natural}$ during accommodation. Group B was composed of subjects ($n = 15$) with decreased $HORMS_{natural}$ during accommodation. In the nonaccommodative state, PD and ASC of Group A were larger than those of Group B (independent *t*-test, $P < 0.05$, Table 3, Fig. 7). However, $HORMS_{fixed}$ and $HORMS_{natural}$ of Group A were smaller than those of Group B (independent t-test, $P < 0.05$, Fig. 8). In the accommodative state, subjects in Group A had larger PD and PSC (independent *t*-test, $P < 0.05$, Table 4, Fig. 7). However, $HORMS_{fixed}$ in Group A was significantly smaller than that in Group B (independent *t*-test, $P < 0.05$, Fig. 8). No differences of $HORMS_{natural}$ were found between the two subgroups (independent *t*-test, $P < 0.05$, Fig. 8). During accommodation, the mean of the increased $HORMS_{natural}$ in Group A was 0.088 ± 0.061 μm, and the mean of the increased $HORMS_{fixed}$ was 0.140 ± 0.078 μm. The mean of the decreased $HORMS_{natural}$ in Group B was 0.052 ± 0.039 μm, and the mean of the increased $HORMS_{fixed}$ was 0.196 ± 0.107 μm.

DISCUSSION

In this study, we investigated the relationship between the anterior segment biometry and the ocular HOAs by using UL-OCT and wavefront sensor. The importance of our study lies in further understanding the optical properties and the mechanism of ocular accommodation. Oberheide et al. (*IOVS* 2012;53:ARVO E-Abstract 1344) combined a commercial OCT (SL-OCT; Heidelberg Engineering GmbH, Heidelberg, Germany) and a ray-tracing aberrometer (iTrace; Tracey Technologies Corp., Houston, TX) to measure simultaneously the wavefront and lens shape of 10 subjects during accommodation. In their study, it was not clear how the anterior segment from the cornea and the entire crystalline lens were measured using their OCT instrument, which had a scan depth of only 7 mm. In addition, Oberheide et al. only reported the measurements, and no relationships between aberrations and anterior segment biometry were given, possibly due to the small sample size. To the best of our knowledge, our current experiments are the first in which the UL-OCT and Hartman-Shack wavefront sensor have been combined to study the relationships between the wavefront measurements and anterior segment biometry during accommodation. The combination of systems was documented in our recent study,[18] and the technical details of the integrated instrument were described.

Accommodation-Related Alterations

The accommodative changes in the biometry and aberrations measured in our study are in agreement with those of previous studies (Table 5).[9,10,27–33] The accommodation-induced dimen-

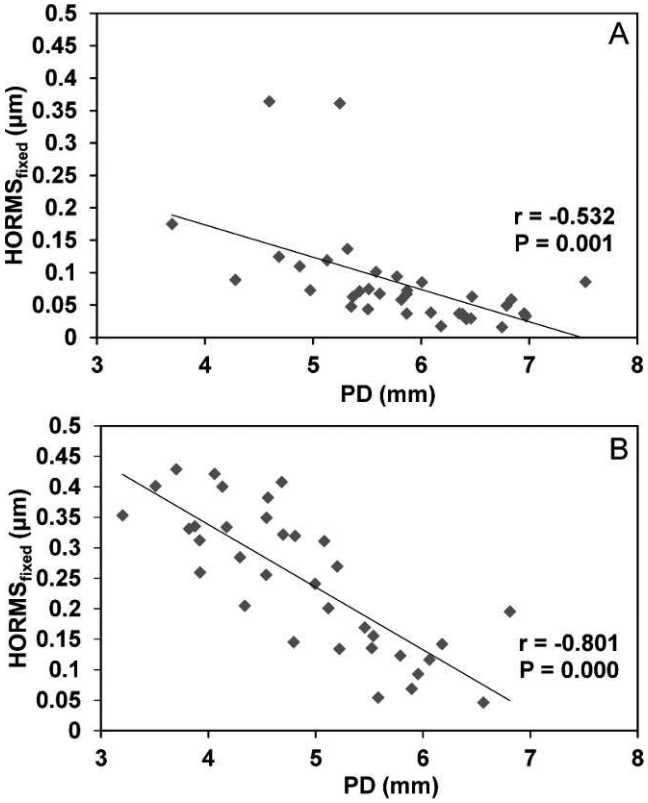

FIGURE 6. Relationships between PD and HORMS$_{fixed}$ in nonaccommodative and accommodative states. There was a negative correlation between the PD and HORMS$_{fixed}$ in (**A**) nonaccommodative and (**B**) accommodative states.

sional alterations in the anterior segment observed in our study support the classic theories by Helmholtz and others, and the results fall well within previously reported ranges. Briefly, the anterior surface of the lens became considerably steeper and moved forward, which led to a shallow anterior chamber and increased lens axial thickness in the accommodated eyes. The posterior surface of the lens also became steeper, but the position of the posterior pole remained unchanged. A similar phenomenon was confirmed using other methods, including magnetic resonance imaging (MRI),[28,34] Scheimpflug photography,[28,35,36] ultrasound biomicroscopy,[37] and Purkinje imaging.[35] However, these methods may have some drawbacks. For instance, MRI has a resolution of only 0.156 mm and a slow scan speed.[28] Moreover, the natural accommodative process

TABLE 3. Comparisons Between Groups A and B Under the Nonaccommodative State

	Group A		Group B		
Variable	Mean	SD	Mean	SD	*P* Value
PD, mm	6.047	0.831	5.440	0.720	0.01*
ACD, mm	3.076	0.264	2.991	0.234	0.17
ASC, mm	12.628	1.160	11.923	1.002	0.03*
PSC, mm	5.872	0.464	5.552	0.879	0.08
LT, mm	3.578	0.173	3.644	0.257	0.18
ASL, mm	6.653	0.266	6.635	0.346	0.43
HORMS$_{natural}$, μm	0.349	0.112	0.494	0.054	<0.001*
HORMS$_{fixed}$, μm	0.059	0.036	0.119	0.103	0.01*

* Statistically significant difference.

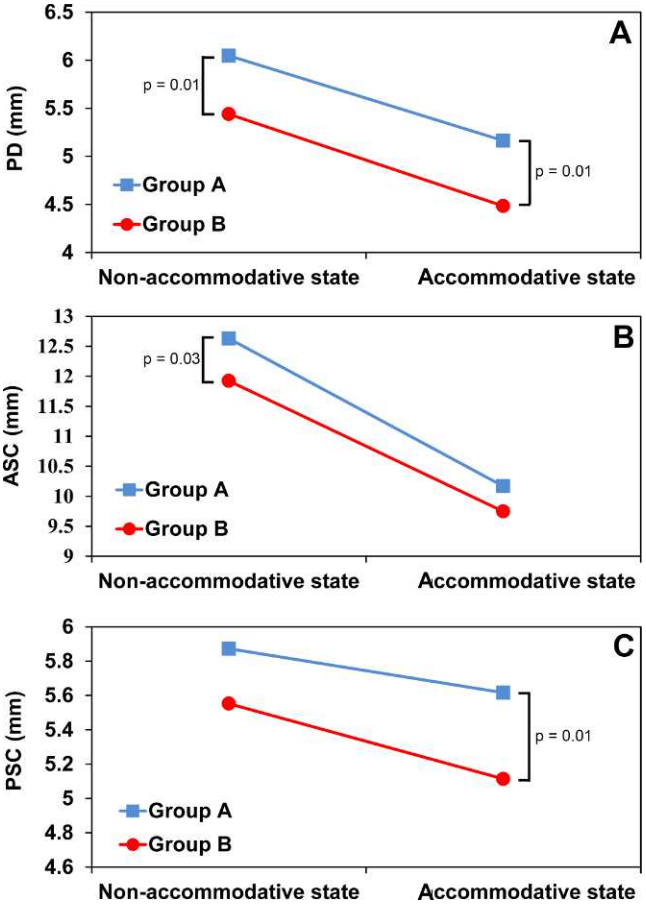

FIGURE 7. Differences in PD (**A**), ASC (**B**), and PSC (**C**) between Groups A and B. Group A consisted of subjects ($n = 20$) with increased HORMS$_{natural}$ during accommodation, and Group B consisted of subjects ($n = 15$) with decreased HORMS$_{natural}$ during accommodation.

may be influenced by the stimulation of visible blue light in Scheimpflug photography[28,35,36] and by contact with a water bath in ultrasound biomicroscopy.[37] The OCT is a noninvasive, rapid, and cross-sectional imaging technology with high resolution and scan speed. The use of near-infrared light makes it possible to maintain the natural accommodative condition during OCT imaging.[14–17]

The HOAs vary with age,[38] refractive error,[39] and pupil size.[30] Additionally, thinning of the tear film contributes to the variation of HOAs.[40] During accommodation, the microfluctuations of pupil size, the ciliary body, and the crystalline lens are

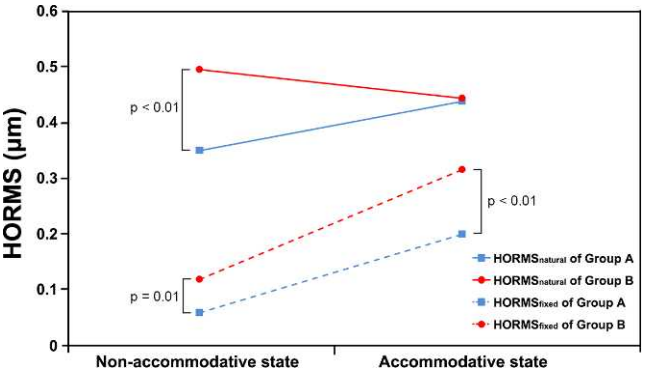

FIGURE 8. Difference in HORMS between Groups A and B.

Table 4. Comparisons Between Groups A and B Under the Accommodative State

Variable	Group A Mean	Group A SD	Group B Mean	Group B SD	*P* Value
PD, mm	5.163	0.864	4.483	0.817	0.01*
ACD, mm	2.954	0.280	2.888	0.222	0.23
ASC, mm	10.168	0.874	9.748	1.035	0.10
PSC, mm	5.616	0.540	5.114	0.758	0.01*
LT, mm	3.700	0.193	3.759	0.257	0.22
ASL, mm	6.653	0.287	6.647	0.333	0.48
$HORMS_{natural}$, μm	0.437	0.094	0.443	0.041	0.41
$HORMS_{fixed}$, μm	0.199	0.096	0.315	0.108	<0.001*

* Statistically significant difference.

well characterized.[41,42] These factors also may result in unstable measurement of HOAs. The Hartmann-Shack wavefront sensor is a highly accurate apparatus for measuring ocular wavefront aberrations,[43] and is used to evaluate optical quality.[44] The increase in HORMS caused by accommodation was consistent with findings of the previous studies (Table 5).

The wavefront sensor readings were used for the measurements of accommodative response. By using Seidel defocus (Equation 1), the wavefront sensor provided a methodology of objective accommodation measurements, which has been well-documented in previous reports.[26,45] In agreement with a previous study,[46] the subjects in the current study tended to overaccommodate for a distant target and underaccommodate for a near target. However, the accommodative lag under near viewing in this study was larger than that in a previous report.[46] This may be explained by the differences in viewing conditions between monocular and binocular measurements, the latter of which allows the accommodation-vergence loop to remain open. Several investigators have found smaller accommodative lag in binocular measurements compared to those during monocular measurements.[47–49]

Relationship Between Ocular Biometry and Optical Properties

In our study, we found a negative correlation between changes in ASC and changes in HOAs during accommodation. This indicated that the steepening of the lens anterior surface contributed significantly to the increase of HOAs. Although the anterior and posterior surfaces are proportional to the diopter power, the change in the shape and power of the anterior surface is much greater than that in the posterior surface.[50] Therefore, the lens anterior surface may be the main factor in the accommodation of the ocular optical system.

Several in vitro experiments also explored the relationship between the biometry and the aberrations.[51,52] Roorda and Glasser speculated that the central curvature of the lens steepens, while the peripheral region becomes flattened, causing the spherical aberration to become increasingly negative.[52] Lopez-Gil and Fernandez-Sanchez considered that the decrease in spherical aberration mainly resulted from the change in the anterior surface of the lens.[53] Moreover, other factors, such as refractive index gradients inside the lens, also may alter aberrations with accommodation.[54] Smith et al. concluded that the surface curvature, refractive index, and asphericity affected spherical aberrations in their schematic human model eye.[51] Importantly, the studies mentioned above were conducted in model eyes or in vitro, while we verified the relationships in human eyes in vivo.

The change of HOAs may be a byproduct of lens changes that add optical power during accommodation. Although the eye is accommodating to compensate for low-order aberrations (mainly defocus) and to improve the retinal image quality during near vision, accommodative lag occurs in most subjects.[55] Considering that more accommodation leads to more HOAs that may reduce retinal image quality, it has been

Table 5. Accommodative-Induced Alteration in Anterior Segment Biometry and Wavefront Aberrations for the Current Study Compared to Other Studies

Variable	Mean Value in Relaxed State and Accommodative Change in Present Study	Mean Value in Relaxed State and Accommodative Change Reported Previously: Relaxed (Accommodative Change)	Image Technology/Reference
ACD	3.040 ± 0.252 mm	3.85 ± 0.07 mm (−0.044 mm/D_{stim})	Ultrasound[33]
	−0.055 ± 0.015 mm/D_{resp}	3.795 ± 0.167 mm (−0.047 mm/D_{resp})	PCI[27]
	−0.038 ± 0.011 mm/D_{stim}	3.79 ± 0.22 mm (−0.24 mm/D_{stim})	OCT[31]
ASC	12.326 ± 1.136 mm	12.15 ± 0.6 mm (−0.64 ± 0.1 mm/D_{resp})	Scheimpflug[28]
	−1.228 ± 0.422 mm/D_{resp}	11.89 ± 2.75 mm (−0.63 ± 0.50 mm/D_{resp})	MRI[32]
	−0.779 ± 0.291 mm/D_{stim}	11.45 ± 1.7 mm (−0.51 ± 0.5 mm/D_{resp})	MRI[28]
PSC	5.735 ± 0.681 mm	5.82 ± 0.6 mm (−0.16 ± 0.1 mm/D_{resp})	Scheimpflug[28]
	−0.148 ± 0.198 mm/D_{resp}	6.12 ± 0.75 mm (−0.15 ± 0.18 mm/D_{resp})	MRI[32]
	−0.116 ± 0.181 mm/D_{stim}	6.11 ± 1.4 mm (−0.14 ± 0.13 mm/D_{resp})	MRI[28]
LT	3.606 ± 0.213 mm	3.74 ± 0.08 mm (+0.051 mm/D_{stim})	Ultrasound[33]
	+0.053 ± 0.027 mm/D_{resp}	3.598 ± 0.230 mm (+0.063 mm/D_{resp})	PCI[27]
	+0.040 ± 0.018 mm/D_{stim}	3.684 ± 0.06 mm (+0.045 mm/D_{resp})	Scheimpflug[28]
		3.66 ± 0.14 mm (+0.061 mm/D_{resp})	MRI[28]
		3.93 ± 0.30 mm (+0.065 mm/D_{resp})	MRI[29]
		3.95 ± 0.30 mm (+0.064 mm/D_{resp})	OCT[29]
HORMS	0.085 ± 0.078 μm (3 mm pupil size)	+0.022 μm/D_{resp} (4-mm pupil size)	Hartmann-Shack aberrometer[9]
	+0.094 ± 0.049 μm/D_{resp}	+0.0837 D/D_{resp}*	Hartmann-Shack aberrometer[10]
	+0.055 ± 0.031 μm/D_{stim}	0.103 ± 0.037 μm (4-mm pupil size)	Hartmann-Shack aberrometer[30]

D_{resp} and D_{stim} are diopters of accommodative response and diopters of stimulus demand, respectively.
* Calculated as the form of equivalent defocus (M).

Investigative Ophthalmology & Visual Science

hypothesized that the presence of accommodative lag could be explained as a balance between defocus and HOAs.[53] The lower level of accommodative response may cause more defocus, but it also would avoid more HOAs being added to eye.

Effect of Pupil Miosis

Pupil size may be another key factor in accommodation. In our study, the HORMS of constant aperture (fixed pupil diameter) significantly increased with accommodation, but HORMS under physiologic pupil size conditions remained unchanged.[56] These results imply that although the ocular HOAs increased due to the dimensional changes of the anterior eye, the contraction of the pupil significantly reduced HOAs during accommodation. Interestingly, the role of the pupil as an aperture diaphragm could be observed even in the nonaccommodative condition. Pupil size was correlated negatively with HORMS for fixed pupil size in accommodative and nonaccommodative states. This phenomenon does not contradict previous findings that HORMS decreased with the pupil miosis for individual subjects.[30] Our findings indicated that in a given population, the eyes having poorer optical quality also had smaller pupil size compared to those with excellent optics. Therefore, the results support rather than oppose the idea that pupil miosis tends to reduce the effect of HOAs and benefits vision by controlling the retinal optical image quality during accommodation. This also may explain why the pupil size is smaller in high myopes and elders whose HOAs are higher than young emmetropes.[57]

Difference Between the Subgroups

Although accommodation-induced reshaping of the lens caused more ocular HOAs, it appeared that the human eye maintained the ability to evaluate the quality of optical images on the retina. In our study, changes in HORMS with accommodation varied greatly among individuals, so the subjects were divided into two subgroups based on the tendencies of changes in HOAs: the subjects in Group A had an increasing $HORMS_{natural}$, while the subjects in Group B had a decreasing $HORMS_{natural}$ during accommodation. The results showed that the lens anterior surface of the subjects in Group A was flatter and had more potential to reshape than in Group B when accommodating, in agreement with Dubbelman et al.[36] We hypothesized that the optical medium quality may be better in Group A compared to that in Group B. Even the lens anterior surface reshaping was greater in Group A, resulting in the lower $HORMS_{fixed}$. Moreover, the pupil size in Group A was relatively larger due to the better ocular optical quality. On the other hand, the subjects with steeper anterior surface of the lens may have poorer ocular optical quality. Thus, the alteration in the lens anterior surface may be smaller during accommodation, accompanied by the reduction of the pupil size, to avoid the occurrence of more HOAs. These phenomena imply the existence of an autoregulatory mechanism that maintains a stable retinal optical image quality, and the HORMS under natural pupil conditions remain unchanged. Several hints on this autoregulatory mechanism have been indicated in the literature.[30,53] The actual mechanism of the regulatory system will need to be clarified by further research.

There are some limitations of this study. First, using the apex of the cornea for positioning the eye may cause an alignment error on the lens, because the lens may have some tilt and decentration, especially during accommodation.[58] Second, the lens surface was measured as a single curve but the actual curvature is complex. Third, the constant refractive index of 1.408 for the crystalline lens was used in image correction. We assumed that the refractive index of the lens remained the same during accommodation. If this assumption is not correct, then it may induce an error in the measurement of the posterior lens surface.

In conclusion, the biometric dimensions of the ocular anterior segment and ocular HOAs changed significantly during accommodation. It appeared that the increase in HOAs was mainly due to the increased convexity of the anterior surface of the crystalline lens during accommodation. Meanwhile, contraction of the pupil during accommodation may help to decrease HOAs. Future studies of the accommodation process using UL-OCT and wavefront sensor may provide more insight into accommodation by the human eye.

Acknowledgments

Supported by research grants from the National Natural Science Foundation of China (Grants 81170869 [FL], 81101081 [DZ], and 81200672 [QC]), National Basic Research (973) Program of China (2011CB504601), and Development Program Project Grant of Wenzhou, China (Y20100296 [AT]). The authors alone are responsible for the content and writing of the paper.

Disclosure: **Y. Yuan**, None; **Y. Shao**, None; **A. Tao**, None; **M. Shen**, None; **J. Wang**, None; **G. Shi**, None; **Q. Chen**, None; **D. Zhu**, None; **Y. Lian**, None; **J. Qu**, None; **Y. Zhang**, None; **F. Lu**, None

References

1. von Helmholtz H. Uber die Akkommodation des Auges. *Archiv Ophthalmol*. 1855;1:1–74.
2. Le R, Bao J, Chen D, He JC, Lu F. The effect of blur adaptation on accommodative response and pupil size during reading. *J Vis*. 2010;10:1.
3. Tsukamoto M, Nakajima K, Nishino J, Hara O, Uozato H, Saishin M. Accommodation causes with-the-rule astigmatism in emmetropes. *Optom Vis Sci*. 2000;77:150–155.
4. Mutti DO, Enlow NL, Mitchell GL. Accommodation and induced with-the-rule astigmatism in emmetropes. *Optom Vis Sci*. 2001;78:6–7.
5. Hazel CA, Cox MJ, Strang NC. Wavefront aberration and its relationship to the accommodative stimulus-response function in myopic subjects. *Optom Vis Sci*. 2003;80:151–158.
6. He JC, Burns SA, Marcos S. Monochromatic aberrations in the accommodated human eye. *Vision Res*. 2000;40:41–48.
7. Atchison DA, Collins MJ, Wildsoet CF, Christensen J, Waterworth MD. Measurement of monochromatic ocular aberrations of human eyes as a function of accommodation by the Howland aberroscope technique. *Vision Res*. 1995;35:313–323.
8. Cheng H, Barnett JK, Vilupuru AS, et al. A population study on changes in wave aberrations with accommodation. *J Vis*. 2004;4:272–280.
9. Lopez-Gil N, Fernandez-Sanchez V, Legras R, Montes-Mico R, Lara F, Nguyen-Khoa JL. Accommodation-related changes in monochromatic aberrations of the human eye as a function of age. *Invest Ophthalmol Vis Sci*. 2008;49:1736–1743.
10. Radhakrishnan H, Charman WN. Age-related changes in ocular aberrations with accommodation. *J Vis*. 2007;7:11–21.
11. Fincham EF. The mechanism of accommodation. *Br J Ophthalmol*. 1937;(suppl 8):7–80.
12. Buehren T, Collins MJ, Loughridge J, Carney LG, Iskander DR. Corneal topography and accommodation. *Cornea*. 2003;22:311–316.
13. He JC, Gwiazda J, Thorn F, Held R, Huang W. Change in corneal shape and corneal wave-front aberrations with accommodation. *J Vis*. 2003;3:456–463.

14. Huang D, Swanson EA, Lin CP, et al. Optical coherence tomography. *Science*. 1991;254:1178–1181.
15. Izatt JA, Hee MR, Swanson EA, et al. Micrometer-scale resolution imaging of the anterior eye in vivo with optical coherence tomography. *Arch Ophthalmol*. 1994;112:1584–1589.
16. Shen M, Cui L, Li M, Zhu D, Wang MR, Wang J. Extended scan depth optical coherence tomography for evaluating ocular surface shape. *J Biomed Opt*. 2011;16:056007.
17. Yuan Y, Chen F, Shen M, Lu F, Wang J. Repeated measurements of the anterior segment during accommodation using long scan depth optical coherence tomography. *Eye Contact Lens*. 2012;38:102–108.
18. Shi G, Wang Y, Yuan Y, Wei L, Lv F, Zhang Y. Measurement of ocular anterior segment dimension and wavefront aberration simultaneously during accommodation. *J Biomed Opt*. 2012;17:120501.
19. Yang JS, Wei L, Chen H, Rao X, Rao C. Absolute calibration of Hartmann-Shack wavefront sensor by spherical wavefronts. *Opt Comm*. 2010;283:910–916.
20. Du C, Wang J, Cui L, Shen M, Yuan Y. Vertical and horizontal corneal epithelial thickness profiles determined by ultrahigh resolution optical coherence tomography. *Cornea*. 2012;31:1036–1043.
21. Du C, Shen M, Li M, Zhu D, Wang MR, Wang J. Anterior segment biometry during accommodation imaged with ultra-long scan depth optical coherence tomography. *Ophthalmology*. 2012;119:2479–2485.
22. Stephen RU, Fabrice M, Hassan T, Pascal R, Jean-Marie P. Corneal group refractive index measurement using low-coherence interferometry. *SPIE*. 1998;3246:14–21.
23. David AA, George S. Chromatic dispersion of the ocular media of human eyes. *J Opt Soc Am A*. 2005;22:29–37.
24. Uhlhorn SR, Borja D, Manns F, Parel JM. Refractive index measurement of the isolated crystalline lens using optical coherence tomography. *Vision Res*. 2008;48:2732–2738.
25. Thibos LN, Applegate RA, Schwiegerling JT, Webb R. Report from the VSIA taskforce on standards for reporting optical aberrations of the eye. *J Refract Surg*. 2000;16:S654–S655.
26. Thibos LN, Hong X, Bradley A, Applegate RA. Accuracy and precision of objective refraction from wavefront aberrations. *J Vis*. 2004;4:329–351.
27. Bolz M, Prinz A, Drexler W, Findl O. Linear relationship of refractive and biometric lenticular changes during accommodation in emmetropic and myopic eyes. *Br J Ophthalmol*. 2007;91:360–365.
28. Hermans EA, Pouwels PJ, Dubbelman M, Kuijer JP, van der Heijde RG, Heethaar RM. Constant volume of the human lens and decrease in surface area of the capsular bag during accommodation: an MRI and Scheimpflug study. *Invest Ophthalmol Vis Sci*. 2009;50:281–289.
29. Richdale K, Sinnott LT, Bullimore MA, et al. Quantification of age-related and per diopter accommodative changes of the lens and ciliary muscle in the emmetropic human eye. *Invest Ophthalmol Vis Sci*. 2013;54:1095–1105.
30. Applegate RA, Donnelly WJ III, Marsack JD, Koenig DE, Pesudovs K. Three-dimensional relationship between high-order root-mean-square wavefront error, pupil diameter, and aging. *J Opt Soc Am A Opt Image Sci Vis*. 2007;24:578–587.
31. Yan PS, Lin HT, Wang QL, Zhang ZP. Anterior segment variations with age and accommodation demonstrated by slit-lamp-adapted optical coherence tomography. *Ophthalmology*. 2010;117:2301–2307.
32. Sheppard AL, Evans CJ, Singh KD, Wolffsohn JS, Dunne MC, Davies LN. Three-dimensional magnetic resonance imaging of the phakic crystalline lens during accommodation. *Invest Ophthalmol Vis Sci*. 2011;52:3689–3697.
33. Storey JK, Rabie EP. Ultrasound—a research tool in the study of accommodation. *Ophthalmic Physiol Opt*. 1983;3:315–320.
34. Kasthurirangan S, Markwell EL, Atchison DA, Pope JM. MRI study of the changes in crystalline lens shape with accommodation and aging in humans. *J Vis*. 2011;11:19, 1–16.
35. Rosales P, Dubbelman M, Marcos S, van der Heijde R. Crystalline lens radii of curvature from Purkinje and Scheimpflug imaging. *J Vis*. 2006;6:1057–1067.
36. Dubbelman M, Van der Heijde GL, Weeber HA. Change in shape of the aging human crystalline lens with accommodation. *Vision Res*. 2005;45:117–132.
37. Liebmann JM, Ritch R. Ultrasound biomicroscopy of the anterior segment. *J Am Optom Assoc*. 1996;67:469–479.
38. Berrio E, Tabernero J, Artal P. Optical aberrations and alignment of the eye with age. *J Vis*. 2010;10:34.
39. Cheng X, Bradley A, Hong X, Thibos LN. Relationship between refractive error and monochromatic aberrations of the eye. *Optom Vis Sci*. 2003;80:43–49.
40. Xu J, Bao J, Deng J, Lu F, He JC. Dynamic changes in ocular Zernike aberrations and tear menisci measured with a wavefront sensor and an anterior segment OCT. *Invest Ophthalmol Vis Sci*. 2011;52:6050–6056.
41. Zhu M, Collins MJ, Robert ID. Microfluctuations of wavefront aberrations of the eye. *Ophthalmic Physiol Opt*. 2004;24:562–571.
42. Schultz KE, Sinnott LT, Mutti DO, Bailey MD. Accommodative fluctuations, lens tension, and ciliary body thickness in children. *Optom Vis Sci*. 2009;86:677–684.
43. Bruno TL, Wirth A, Jankevics AJ. Applying Hartmann wavefront-sensing technology to precision optical testing of the Hubble Space Telescope correctors. *Proc. SPIE 1920, Active and Adaptive Optical Components and Systems II, 328*. August 25, 1993. doi:10.1117/12.152677.
44. Liang J, Grimm B, Goelz S, Bille JF. Objective measurement of wave aberrations of the human eye with the use of a Hartmann-Shack wave-front sensor. *J Opt Soc Am A Opt Image Sci Vis*. 1994;11:1949–1957.
45. Tarrant J, Roorda A, Wildsoet CF. Determining the accommodative response from wavefront aberrations. *J Vis*. 2010;10:4.
46. Charman WN. The eye in focus: accommodation and presbyopia. *Clin Exp Optom*. 2008;91:207–225.
47. Manny RE, Chandler DL, Scheiman MM, et al. Accommodative lag by autorefraction and two dynamic retinoscopy methods. *Optom Vis Sci*. 2009;86:233–243.
48. Nakatsuka C, Hasebe S, Nonaka F, Ohtsuki H. Accommodative lag under habitual seeing conditions: comparison between adult myopes and emmetropes. *Jpn J Ophthalmol*. 2003;47:291–298.
49. Jiang BC, Tea YC, O'Donnell D. Changes in accommodative and vergence responses when viewing through near addition lenses. *Optometry*. 2007;78:129–134.
50. Garner LF, Yap MK. Changes in ocular dimensions and refraction with accommodation. *Ophthalmic Physiol Opt*. 1997;17:12–17.
51. Smith G, Bedggood P, Ashman R, Daaboul M, Metha A. Exploring ocular aberrations with a schematic human eye model. *Optom Vis Sci*. 2008;85:330–340.
52. Roorda A, Glasser A. Wave aberrations of the isolated crystalline lens. *J Vis*. 2004;4:250–261.
53. Lopez-Gil N, Fernandez-Sanchez V. The change of spherical aberration during accommodation and its effect on the accommodation response. *J Vis*. 2010;10:12.
54. Navarro R, Palos F, Gonzalez LM. Adaptive model of the gradient index of the human lens. II. Optics of the accommodating aging lens. *J Opt Soc Am A Opt Image Sci Vis*. 2007;24:2911–2920.

Investigative Ophthalmology & Visual Science

55. Anderson HA, Glasser A, Stuebing KK, Manny RE. Minus lens stimulated accommodative lag as a function of age. *Optom Vis Sci*. 2009;86:685–694.

56. Li YJ, Choi JA, Kim H, Yu SY, Joo CK. Changes in ocular wavefront aberrations and retinal image quality with objective accommodation. *J Cataract Refract Surg*. 2011;37:835–841.

57. Alfonso JF, Ferrer-Blasco T, Gonzalez-Meijome JM, Garcia-Manjarres M, Peixoto-de-Matos SC, Montes-Mico R. Pupil size, white-to-white corneal diameter, and anterior chamber depth in patients with myopia. *J Refract Surg*. 2010;26:891–898.

58. Ruggeri M, Uhlhorn SR, De FC, Ho A, Manns F, Parel JM. Imaging and full-length biometry of the eye during accommodation using spectral domain OCT with an optical switch. *Biomed Opt Express*. 2012;3:1506–1520.

Investigative Ophthalmology & Visual Science